13th International Symposium on Particle Image Velocimetry – ISPIV 2019
Munich, Germany, July 22-24, 2019

# Stereoscopic PTV measurements in the housing/rotor cavity of a shrouded turbine rotor

**Rainer Hain[1*], Thomas Fuchs[1], Lars Wein[2], Tim Kluge[2], Jörg Seume[2], Christian J. Kähler[1]**

[1] Universität der Bundeswehr München, Institute of Fluid Mechanics and Aerodynamics, Neubiberg, Germany

[2] Leibniz Universität Hannover, Institute of Turbomachinery and Fluid Dynamics, Hannover, Germany

[*] rainer.hain@unibw.de

## Abstract

Particle Image Velocimetry and Particle Tracking Velocimetry are well established measurement techniques for the acquisition of velocity fields in transparent fluids. Due to the scalability, these techniques are applicable for micro- and macro-flows as well as for low- and high-speed flows. For macroscopic measurements in air typically liquid fluids are used for the generation of seeding particles. Often fluids such as vegetable oils or DEHS are atomized in Laskin nozzle generators resulting in particles with a mean diameter on the order of 1 µm. Similar sized tracer particles are generated using fog generators operated with water-glycol mixtures. In many flows, particles with such a diameter and density show a nearly perfect following behavior. However, if high accelerations occur, the path-lines of the particles deviate from the stream-lines of the flow. This deviation may affect the measurement accuracy and particles can deposit on walls, and thus the optical access might be impaired. In this paper we will analyze the contamination problems occurring in a high-speed cavity flow and we will present solutions that make high-quality PIV/PTV measurements in such flow environments possible.

## 1 Introduction

Low-pressure turbine blades in engines are often quite long and therefore sensitive to vibration excitations. In order to decrease vibrations and blade deformations, a shroud is attached to the outer side of the blade, see Bräunling (2013). From the aerodynamical view this has the benefit that tip vortices do not occur. However, the rotating shroud may never directly touch the casing in order to avoid a fatal mechanical damage. Therefore, in typical constructions sealing fins are fixed on the outer side of the shroud and on the inside of the casing abrasive coatings or honeycombs are used. In the unlike event of a contact of these elements, no severe damage will occur. However, due to this construction, a gap between the sealing fins and the abrasive coating on the order of $O(1\,\mathrm{mm})$ exists under normal operating conditions, see Ghaffari and Willinger (2013); Gao et al. (2013); Bräunling (2013). This gap allows for a leakage flow resulting in a reduced efficiency of the turbine stage due to mixing losses and increased incidence on the downstream vanes. Biester et al. (2012) showed that the isentropic efficiency of a low pressure turbine stage, similar to those of aero engines, is reduced by 2.5% by the leakage through hub and shroud labyrinth seals. Thus, it is important to understand the flow physics in this region with the aim to lower this leakage flow and to increase the turbine efficiency. A sketch of a typical set-up is given in Fig. 1.

Numerical simulations of these labyrinth seals consisting of the inlet and outlet cavities and the flow over the sealing fins are difficult to perform and the results are often not very accurate for different reasons, Tyacke and Tucker (2014); Wein et al. (2017); Kluge et al. (2019). One reason is the range of scales: Rather large structures can be found in the inflow domain and in the cavities, whereas the flow structures in the gap area are much smaller on average. Another reason is the three dimensionality of the flow and the complexity of the flow physics. Several detachment and reattachment locations occur which are hard to determine by means of industrially relevant numerical methods, i.e. solutions of the Reynolds-Averaged-Navier-Stokes equations with eddy viscosity turbulence models. Typically, those models struggle to accurately predict the

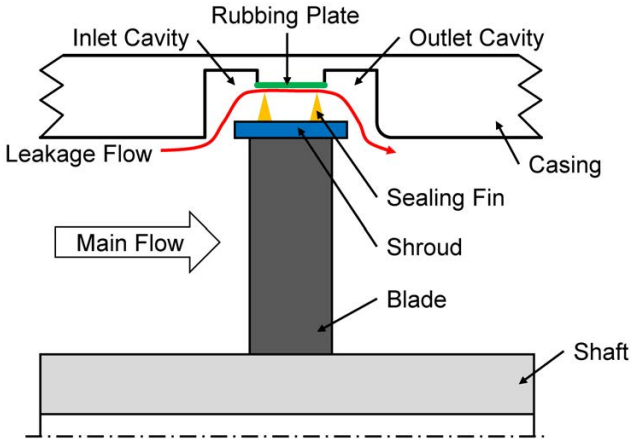


Figure 1: Sketch of a labyrinth sealing in an axial turbine.

flow in labyrinth seals, Tyacke and Tucker (2014); Kluge et al. (2019). The simulation of very thin shear layers and the turbulence production within these shear layers is another challenge. Due to these difficulties, experimental data is required in order to validate numerical simulations. Using pressure probes is difficult in these geometries, since the probes and the flow domains are of similar size. A strong influence of the probes on the flow field can be expected, which is also the case for hot wires. Therefore, the non-intrusive Particle Image Velocimetry (PIV) or Particle Tracking Velocimetry (PTV) techniques are more suitable for these confined geometries. No disturbances are introduced and the velocity distribution as well as statistical data in a plane are captured within a short measurement time. Using stereoscopic PIV/PTV, all three velocity components are obtained. However, the challenges which were mentioned for the simulations partially also hold for the PIV/PTV measurements. The high dynamic velocity range as well as the high dynamic spatial range are challenging (see Adrian (1997) and Keane and Adrian (1990)). Furthermore, large accelerations can cause problems, as outlined by Hain and Kähler (2007).

A basic assumption for particle imaging techniques is a good particle following behavior. For low-speed flows with moderate accelerations this is nearly ideally true. However, the larger the accelerations are, the higher the particle lag is. The velocity lag $U_S$ of a tiny tracer particle in a continuously accelerated flow can be approximated by (see Raffel et al. (2018))

$$\mathbf{U}_S = \mathbf{U}_p - \mathbf{U} = d_p^2 \frac{(\rho_p - \rho)}{18\mu}\mathbf{a}, \tag{1}$$

with the particle velocity $\mathbf{U}_p$, the fluid velocity $\mathbf{U}$, the particle diameter $d_p$, the particle density $\rho_p$, the fluid density $\rho$, the dynamic viscosity $\mu$, and the acceleration $\mathbf{a}$. Bold symbols denote vectors. Please note that a more sophisticated analysis of the velocity lag is given in Adrian and Westerweel (2011). For measurements in air, the particle density $\rho_p$ is approximately three orders of magnitude larger than the gas density $\rho$. According to eq. 1, a smaller velocity lag can only be achieved by using particles with a smaller diameter $d_p$ for a given density and a given acceleration. However, the visibility of particles at $d_p \ll \lambda$ ($\lambda$: wave length of incident light/laser) is limited, since the scattered light intensity strongly decreases with decreasing particle diameter, see Raffel et al. (2018). As a compromise of a low velocity lag and a good visibility, particles for measurements in air typically have a diameter of $d_p \approx 1\,\mu$m and are made from vegetable oil or DEHS (Di-Ethyl-Hexyl-Sebacic-Acid-Ester) which makes them harmless to health and which are easy to generate, see Kähler et al. (2002). The velocity lag is given for a variety of particle sizes/diameters in Fig. 2 for particles made from DEHS in air at standard conditions.

Obviously, particles with $d_p \geq 5\,\mu$m are not suitable for most technical applications, where relatively large flow velocities can be expected. The settling speed of particles in still air can be determined from this figure at $a = g \approx 10\,\mathrm{m/s^2}$. Assuming a wind tunnel with a horizontal measurement section, the settling speed is superimposed on the vertical velocity component which results in a systematic error. However, for DEHS particles with $d_p = 1\,\mu$m the settling speed is only $U_S \approx 3 \cdot 10^{-5}\,\mathrm{m/s} = 0.03\,\mathrm{mm/s}$ and it is therefore negligible for many applications.

In fluid mechanics, large accelerations occur, for instance, when the streamline curvature is high. This might lead to deviations of the streamlines and the path lines of the particles. In a steady flow with $d\mathbf{U}/dt = 0$ and $d_p \to 0$ they would collapse. However, depending on the particle diameter, more or less significant

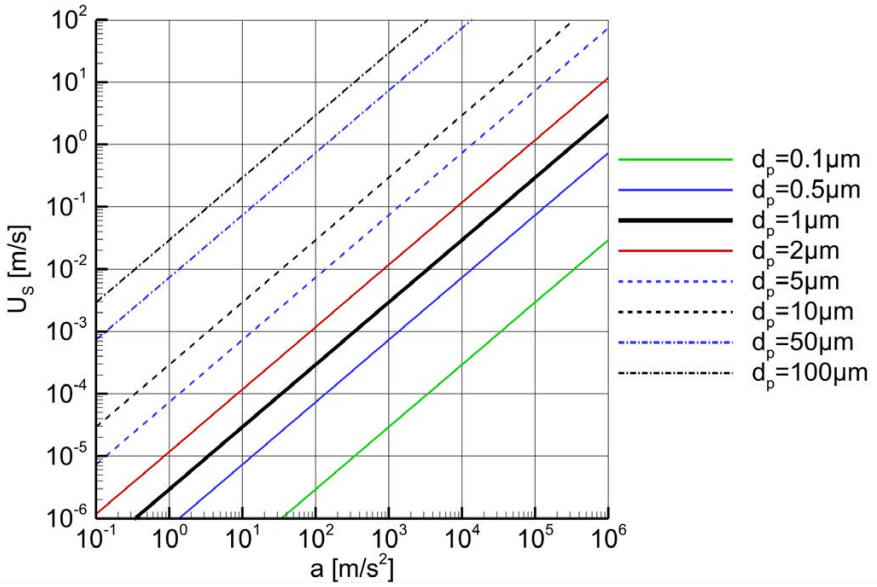


Figure 2: Velocity lag after eq. 1 for $\rho_p = 900\,\mathrm{kg/m^3}$, $\rho = 1.2\,\mathrm{kg/m^3}$ and $\mu = 1.7e-5\,\mathrm{Pa\cdot s}$. A one-dimensional problem with constant acceleration $a$ is assumed.

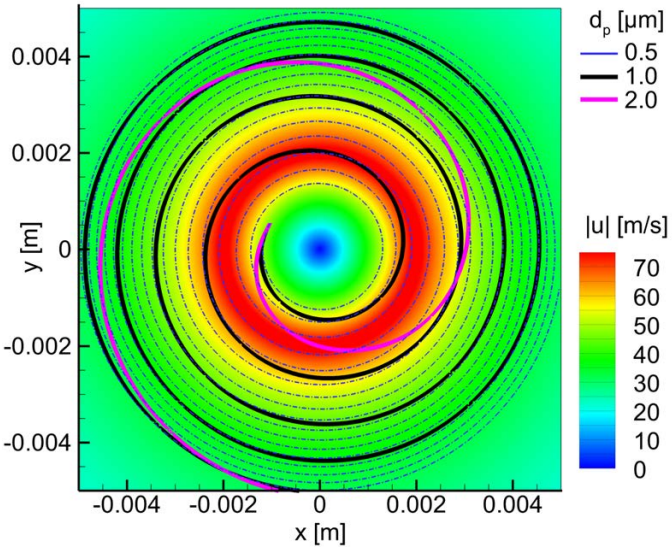


Figure 3: Paths of DEHS particles with diameters $d_p = [0.5;\ 1.0;\ 2.0]\,\mu\mathrm{m}$ in a Rankine vortex with $R = 2\,\mathrm{mm}$ and $\Gamma = 1\,\mathrm{m^2/s}$ for air at standard conditions. Paths have been calculated with Tecplot.

deviations can be observed. Path lines of DEHS particles with diameters $d_p = [0.5;\ 1.0;\ 2.0]\,\mu\mathrm{m}$ in a Rankine vortex with $R = 2\,\mathrm{mm}$ and $\Gamma = 1\,\mathrm{m^2/s}$ for air at standard conditions are shown in Fig. 3.

While a $0.5\,\mu\mathrm{m}$ particle almost ideally follows the theoretical streamlines (which are circles for this flow), the deviation for the $2\,\mu\mathrm{m}$ particle becomes much larger. However, for the accuracy of the measurements the deviation of the streamlines is of little interest. What is more important is the velocity deviation of a particle at a certain location compared to the fluid velocity at that location. Such a comparison for the total velocity as well as the flow angle is shown in Fig. 4 for the trajectories from Fig. 3. Due to the inertia of the particles, the velocity peaks of the Rankine vortex are not captured. In addition, a phase lag occurs and the particle flow angle deviates from the exact flow angle. Naturally, the deviations become higher with increasing particle size.

By looking at Fig. 2 the question arises of how large accelerations in typical flows are. Assuming a steady flow, the remaining acceleration is the convective one. In order to get an impression of the occurring accelerations, Fig. 5 shows the acceleration as a function of $\Delta x$ and $\Delta u$ for three different velocities $u_0$. In this figure, $\Delta x$ is the length of the path of uniform acceleration, $\Delta u$ is the increase in velocity over this path, and $u_0$ is the velocity at the beginning of the acceleration.

This figure demonstrates that very high accelerations can be present in any flow. It is not uncommon that a flow is accelerated by $\Delta u = O(10\,\mathrm{m/s})$ within $\Delta x = O(0.01\,\mathrm{m})$ which results in accelerations around

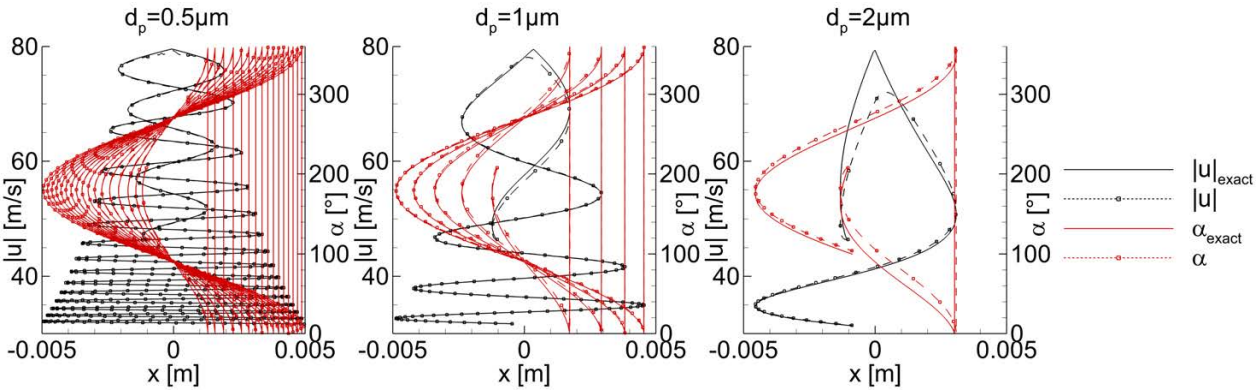


Figure 4: Comparison of particle velocities and angles and the exact quantities of the flow field. Particle paths and simulation parameters are given in Fig. 3.

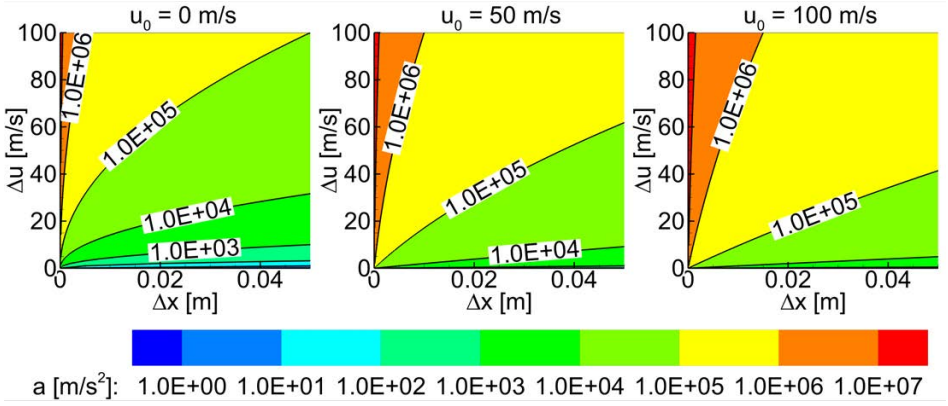


Figure 5: Convective accelerations as functions of $\Delta x$ and $\Delta u$ for three different velocities $u_0$. $\Delta x$ is the path over which the uniform acceleration takes place, $\Delta u$ is the increase in velocity over this path, and $u_0$ is the velocity at the beginning of the acceleration.

$a = O(10^4 - 10^5\,\mathrm{m/s^2})$. Even larger accelerations appear over shock waves. Ragni et al. (2011) have analyzed the particle tracer response for this special flow phenomenon in detail. A velocity lag as mentioned above leads to a measurement error, see Fig. 2. Moreover, particles might accumulate in certain regions. Besides a systematic bias this may also cause problems due to the deposition of particles on the walls. This deposition might change the flow due to the geometry modification and it might worsen the optical access if the affected wall is made from glass and serves as an optical access. Such a construction was used for the flow field measurements in the cavities: Parts of the casing contain flush mounted glass windows in order to allow for the illumination by means of a laser light-sheet and the viewing by means of two cameras for stereoscopic PIV/PTV.

# 2 Experiments

## 2.1 Seeding test facility

In order to investigate different seeding particles and their behavior, a seeding test was devised. The seeding test is a simplified quasi 2D geometry with a small mass flow rate such that it can be operated with the compressed air supply of the workshop. The goal of the investigations was to understand the flow features in the region of the labyrinth seal as well as the seeding particle agglomeration at the walls. This knowledge information will be useful for the investigations in a more sophisticated rotating labyrinth seal test facility offering only a limited optical access, described in detail by Kluge et al. (2019). It has the same dimensions and flow conditions as labyrinth seals of shrouded low pressure turbines like the one investigated by Biester et al. (2012). Although the seeding test is non-axissymmetric, does not capture the rotation of the shroud, and has a lower leakage mass flow rate, the drop of pressure due to the seal fins and the vortex systems in the cavities matches the rotating labyrinth seal test facility. Therefore, similar challenges for PIV/PTV-Measurements can be expected.

In preparation of the experiments, numerical simulations were performed. The set-up for the numerical simulations which is similar to the experimentally investigated seeding test is given in Fig. 6. Steady state RANS-Simulations where carried out using ANSYS-CFX 18 and the Menter SST turbulence model. Details of the setup, the spatial discretization, and numerical sensitivities are given in Kluge et al. (2019). The continuous phase was modeled as an ideal gas while the seeding was modeled as a disperse phase using the Lagrange-Particle tracking approach Ansys (2009). For the disperse phase a homogeneous distribution of spherical DEHS particles with a size of 1 µm at the inlet was defined. No particle breakup, agglomeration, or formation of liquid films due to wall-impact of seeding was modeled. Any particle which impinges the walls is reflected with the same angle. The contour colors in Fig. 6 represent the pressure distribution obtained by means of a numerical simulation. Obviously, high pressure gradients occur in the region of the sealing fins. This is due to the small gaps on the order of 1 mm between the sealing fins and the casing. The seeding volume fraction in the mid-plane of the test facility is shown in Fig. 7. The simulation shows that the seeding concentration in the cavities should be quite small, while in the region of the rounded outlet a high seeding concentration is expected. However, analyzing the momentum transport in Fig. 8 shows, that seeding impinges the walls after flowing through the throttles. The acceleration of the flow and the streamline curvature is too strong and causes a deviation of the particle path from the streamlines of the continuous phase. Since the formation of liquid films and particle agglomeration is not modelled, the consequences of the wall impact of seeding is not captured by the CFD. Nevertheless, it clearly shows the challenges of the flow in labyrinth seals for successful PIV/PTV measurements.

The experimental investigation by means of oil flow visualization shows the result given in Fig. 9. Prior to the investigation, an oil-titanium-oxide paint was applied on the hub and the shroud. After running the facility it is observed that large amounts of the paint are located at the outer case, which was made from transparent polyacrilat windows. Region "A" corresponds to the abrasive coating in the real facility. A contamination is observed beginning at the location of the first sealing fin. This is in good agreement with the prediction of the CFD-Model. Due to the high curvature/acceleration in this region, the paint cannot follow the streamlines and the paint is thrown against the wall. Interestingly, area "B" is also polluted. The CFD-Model shows only minor pollution in this region. However, since the laser illumination as well as the observation of the measurement plane is done through this surface, this pollution is a serious problem, since the optical quality of particle images becomes extremely worse, not allowing for a proper PIV/PTV evaluation.

Investigations with DEHS seeding showed similar results – the surface "B" is contaminated within a short time span ($t = O(10^0 - 10^1\,\mathrm{s})$. An image is not shown here, since the transparent fluid is hard to see on the photo.

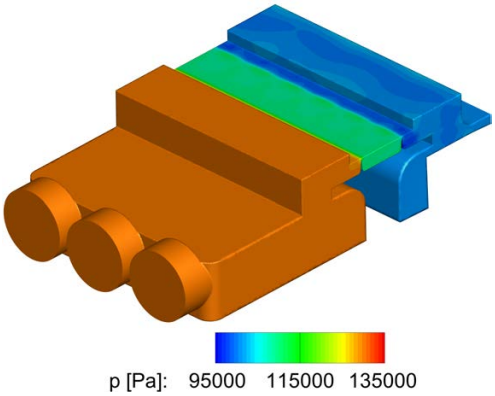


Figure 6: Wall static pressure in the seeding test obtained by means of numerical simulations.

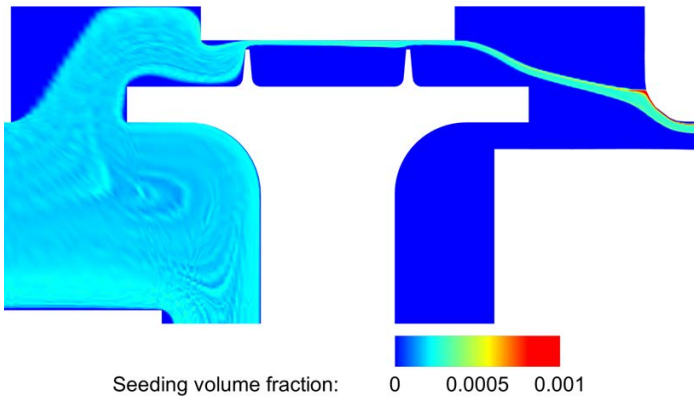


Figure 7: Seeding volume fraction in the mid-plane of the seeding test obtained by means of a numerical simulation.

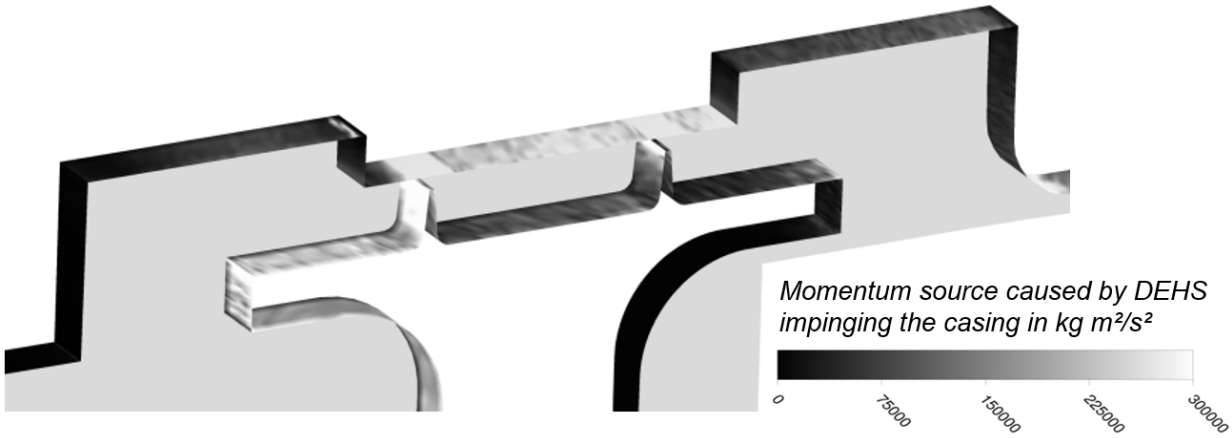


Figure 8: Momentum transfer from DEHS to solid walls in the computational domain.

In order to get a proper optical access, several variations of the geometry in the region of the labyrinth sealing were investigated in the seeding test. However, it has to be kept in mind that the geometry must also work in the real turbine test facility. The geometry which allows for the optical access and which is also suitable for the real facility is shown in Fig. 10. The backward facing step in the outflow cavity is removed by a slight geometry modification. Due to the tangential junction a flow separation is avoided and the flow velocity near the wall/the wall shear stress is quite high which removes the contamination to some extent. The gain of the quality of the recordings will be shown in the next section.

## 2.2 Rotating labyrinth seal test facility

In order to achieve a realistic flow in the region of the shroud and the cavities, a rotating labyrinth seal test facility was designed and build. The facility consists of an outer housing and an inner hub with an annular gap on the order of $10^{-2}$ m. The flow in the annular gap gets a swirl at the inlet by means of a swirl generator and a rotating disc simulates the rotating shroud. The mass flow rate in the shroud region as well as the geometry of the shroud region is similar to the real geometry of the turbine test rig which will be applied for the final investigations. Therefore, the flow features are comparable. However, the rotating labyrinth test facility allows for a more accurate determination of the flow in the shroud region, since it is equipped with many conventional pressure taps and an accurate mass flow meter. A detailed description of the rig and the conventional instrumentation concept is given in Kluge et al. (2019). In addition, the optical access is somewhat better compared with the turbine test rig.

Due to the limited optical access and the high effort to assemble and disassemble the facility, no oil flow visualizations were performed in the rotating labyrinth seal test facility. Data were obtained by means of pressure measurements, which are outside the scope of this paper. However, velocity field measurements were obtained by means of stereoscopic PIV/PTV. A curved glass window with a thickness of 8 mm in the housing allows for the optical access for the cameras and the laser light-sheet was also coupled into the measurement domain through this window. A PIV raw image is shown in Fig. 11(a) for the configuration with the backward facing step in the outflow cavity and Fig. 11(b) shows a raw image for the modified geometry.

The laser light sheet reflections on different surfaces are visible in these figures. Especially, the reflections at the shroud "B" and the hub "C" cross-fade a large area in Fig. 11(a). One reason is the pollution of these surfaces by the seeding which leads to a diffuse reflection of the laser light sheet. The other reason is the deposit of the seeding on the glass which serves as an optical access. Due to this deposit the reflection does not appear sharp in the image anymore - the reflection is smeared out in the direction of the seeding deposit. Since the optical access remains clean to a large extend, the reflections "B" and "C" appear much more focused in Fig. 11(b). This also results in particle images with a better quality as can be observed in Figs. 12(a) and 12(b). Single particle images can clearly be seen in the recordings obtained with the modified geometry. This is not the case for the initial geometry where the surface is highly polluted by the seeding fluid.

To yield sufficient statistical data of the measured flow field, a number of independent measurements on the order of $N = O(10^3)$ is required. The recordings were performed with a rate of $f \approx 10\,s^{-1}$ resulting in an acquisition time of $t = O(10^2)$ s. For the data evaluation two different techniques can be used: 1. PIV and 2. PTV. PIV requires a particle image density which is about $5-10$ times higher than the particle image density

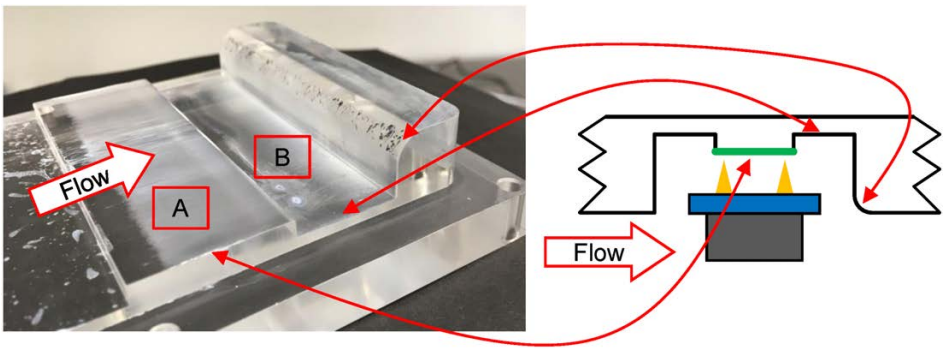


Figure 9: Oil flow visualization in the seeding test.

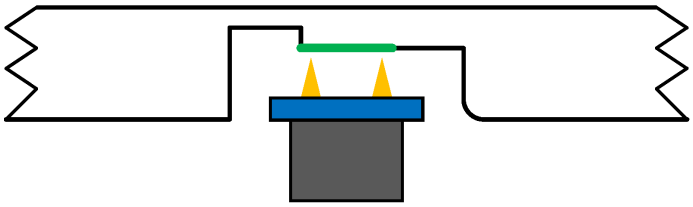

Figure 10: Modified geometry of the outflow region in order to reduce seeding deposition.

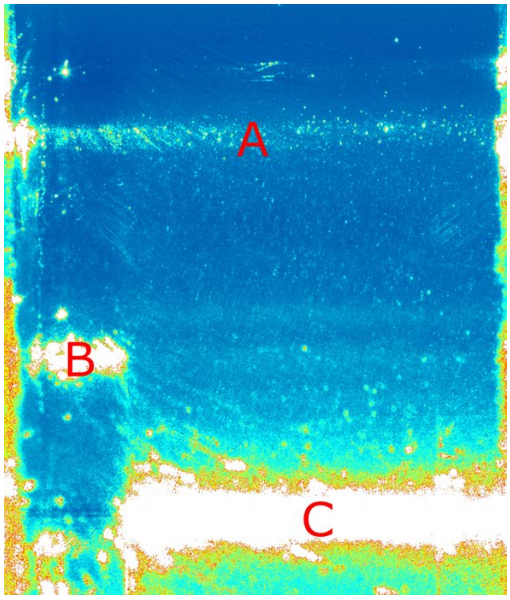


(a) Rotating labyrinth test facility with the original geometry. Due to the seeding deposit on the optical access glass the particle images are blurry.

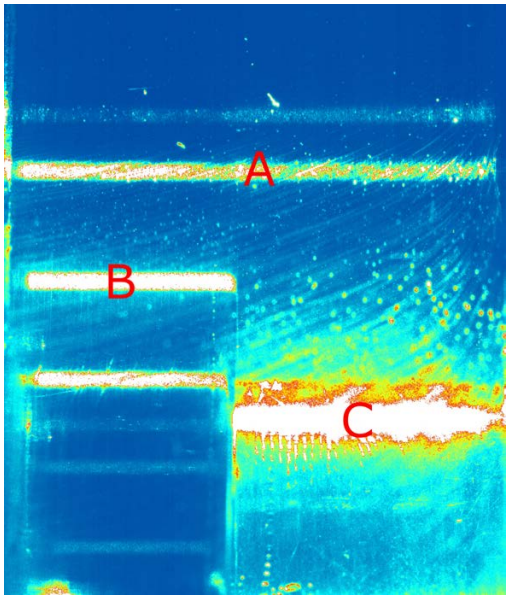


(b) Rotating labyrinth seal test facility with the modified geometry.

Figure 11: Raw images. A: Reflection of the laser light sheet on the inner side of the glass. B: Laser reflection on the shroud. C: Laser reflection on the hub.

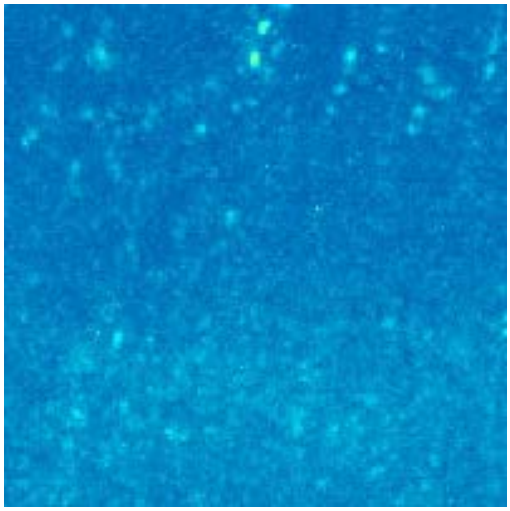

(a) Rotating labyrinth seal test facility with the original geometry.

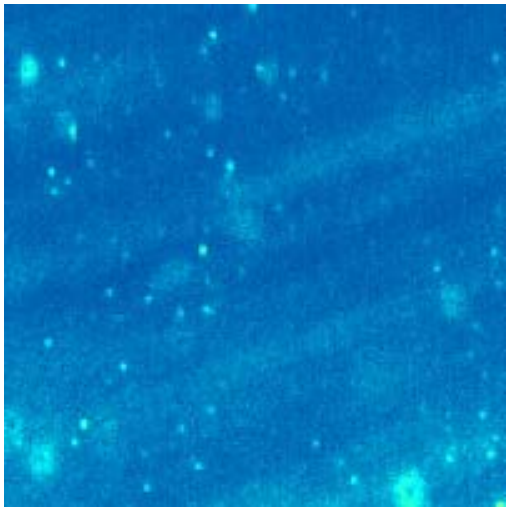

(b) Rotating labyrinth seal test facility with the modified geometry.

Figure 12: Details of the raw images.

for PTV to achieve a comparable spatial resolution. This is a drawback, since this higher seeding density leads to a higher pollution of the facility. Note that the contamination appears not to increase linearly with the seeding concentration. At large seeding concentrations, the pollution appeared faster and more severe, whereas for rather moderate seeding concentrations an almost stationary contamination could be achieved.

Another disadvantage of PIV is the averaging effect due the finite interrogation window size which especially becomes important when small flow structures and high velocity gradients are present. For these two reasons the seeding density was reduced and a PTV evaluation was performed.

A resulting mean velocity field averaged from $\approx 3000$ instantaneous fields is shown in Fig. 13. For the calculation of the statistical values a binning on a regular grid was performed. The Reynolds shear stresses $Re_{uv}$ given in Fig. 14 also show a smooth contour.

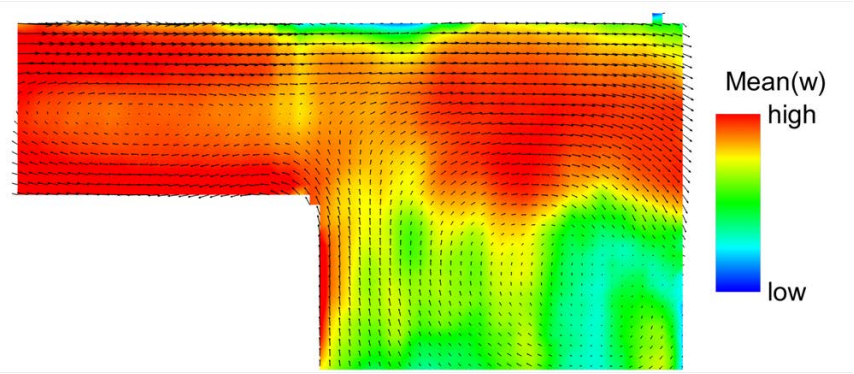


Figure 13: 2D3C velocity field obtained from stereoscopic PTV measurements for the modified geometry. The vectors show the average in-plane velocities and directions. Color coded is the average out-of-plane velocity component.

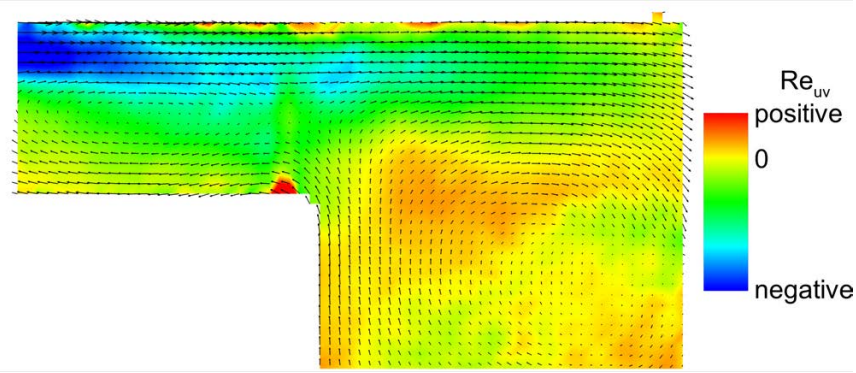


Figure 14: The contour color shows the Reynolds shear stress $\overline{u'v'}$. The vectors show the average in-plane velocities and directions.

## 3 Summary and Conclusion

In industrial environments, applying off-the-shelf particle imaging evaluation becomes difficult quickly due to the complexity of the geometry and flow motion. Due to the flow conditions, seeding particle behavior becomes often critical. Furthermore optical access to the often confined geometries is usually limited. In the presence of large acceleration, small flow structures appear which are difficult to capture with PIV, where spatial averaging underestimates the gradients. Another impediment is the contamination of the walls of the test facilities with depositing seeding particles. In this investigation, where the flow in the cavity region between the housing and the shrouded turbine rotor was measured, the aforementioned difficulties were overcome by different measures. A slight redesign of the housing region suppressed a large separation region downstream of the shroud cavity. As the data serves for validating numerical flow simulations, this

modification is tolerable as without modification, no data could be collected at all. This yielded a significantly reduced pollution of the windows used for the optical access. Furthermore, it was shown that seeding concentrations that are necessary to conduct a cross-correlation evaluation were not feasible because the windows were quickly contaminated, within less than a minute, such that no seeding particles were visible anymore. However, if the seeding concentration was sufficiently low, a stationary contamination level could be reached, ensuring sufficiently long measurement times at multiple operating points. A PTV evaluation of the data yielded average velocity fields and statistical quantities with high spatial resolution. The investigation presented in this text clearly shows that to measure complex flows in challenging environments requires a strong adaptability of the experimental set-up as well as the evaluation techniques to reach the measurement goals. Besides this, Lagrange particle tracking simulations of the DEHS showed similar trends as the oil flow visualization. So, the method has the potential to identify the critical regions in any experimental setup with increased pollution of walls and optical accesses.

## References


Adrian R (1997) Dynamic ranges of velocity andspatial resolution of particle image velocimetry. *Measurement Science and Technology* 8:1393–1398

Adrian RJ and Westerweel J (2011) *Particle Image Velocimetry*. Cambridge University Press, Cambridge, United Kingdom

Ansys (2009) *ANSYS Academic Research, Release 18.1, Help System, ANSYS, Inc*

Biester M, Henke M, Seume JR, Gündogdu Y, and Engel K (2012) Unsteady Wake-Blade Interaction: A Correlation between Surface Pressure Fluctuations and Loss Generation. in *Proceedings of ASME Turbo Expo*. GT2012-69616. Kopenhagen, Denmark

Bräunling WJG (2013) *Flugzeugtriebwerke*. Springer Verlag, Berlin Heidelberg, Germany

Gao J, Zhang H, and Chen H (2013) Comparative investigation of tip leakage flow and its effect on stage performance in shrouded and unshrouded turbines. Proceedings of the Institution of Mechanical Engineers, Part G: Journal of Aerospace Engineering

Ghaffari P and Willinger R (2013) Impact of tip-injection on the performance of partially shrouded turbines: Basic concept and preliminary results. Proceedings of the ASME 2013 Turbine Blade Tip Symposium and Course Week

Hain R and Kähler CJ (2007) Fundamentals of multiframe particle image velocimetry (piv). *Experiments in Fluids* 42:575–587

Kähler CJ, Sammler B, and Kompenhans J (2002) Generation and control of tracer particles for optical flow investigations in air. *Experiments in Fluids* 33:736–742

Keane R and Adrian R (1990) Optimization of particle image velocimeters. Part I: Double pulsed systems.. *Measurement Science and Technology* 1:1202–1215

Kluge T, Wein L, Schmierer R, and Seume JR (2019) Sensitivity analysis, instrumentation and design, and experimental validation of a novel labyrinth seal rig: Etc2019-078. Proceedings of 13th European Conference on Turbomachinery Fluid dynamics and Thermodynamics. Lausanne, Switzerland

Raffel M, Willert CE, Scarano F, Kähler CJ, Wereley ST, and Kompenhans J (2018) *Particle Image Velocimetry*. Springer International Publishing AG, Cham, Switzerland. 3rd edition

Ragni D, Schrijer F, van Oudheusden B, and Scarano F (2011) Particle tracer response across shocks measured by PIV. *Experiments in Fluids* 50:53–64

Tyacke J and Tucker P (2014) Future use of large eddy simulation in aeroengines. *J Turbomach* Published online December 01, 2014. doi:10.1115/1.4029363

Wein L, Seume JR, and Herbst F (2017) Improved prediction of labyrinth seal performance through scale adaptive simulation and stream aligned grids: Gt2017-64257. Proceedings of ASME Turbo Expo 2017. Charlotte, United States of America